



**HAL**  
open science

# Exploring the impact of successive redox events in thin films of Metal-Organic Frameworks: an absorptiometric approach

Vincent Monnier, Fabrice Odobel, Stéphane Diring

## ► To cite this version:

Vincent Monnier, Fabrice Odobel, Stéphane Diring. Exploring the impact of successive redox events in thin films of Metal-Organic Frameworks: an absorptiometric approach. *Journal of the American Chemical Society*, 2023, 145 (35), pp.19232-19242. 10.1021/jacs.3c04114 . hal-04235520

**HAL Id: hal-04235520**

**<https://hal.science/hal-04235520>**

Submitted on 10 Oct 2023

**HAL** is a multi-disciplinary open access archive for the deposit and dissemination of scientific research documents, whether they are published or not. The documents may come from teaching and research institutions in France or abroad, or from public or private research centers.

L'archive ouverte pluridisciplinaire **HAL**, est destinée au dépôt et à la diffusion de documents scientifiques de niveau recherche, publiés ou non, émanant des établissements d'enseignement et de recherche français ou étrangers, des laboratoires publics ou privés.

# Exploring the impact of successive redox events in thin films of Metal-Organic Frameworks: an absorptiometric approach

Vincent Monnier\*, Fabrice Odobel and Stéphane Diring\*

Nantes Université, CNRS, CEISAM, UMR 6230, F-44000 Nantes, France

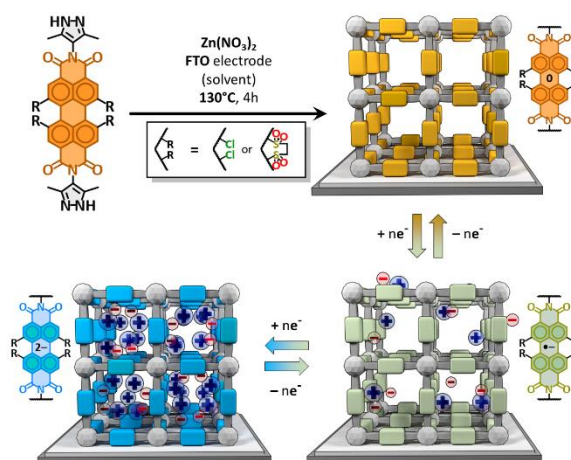
*Metal-Organic Framework, charge diffusion, electrochromism, electrochemistry, MOF-modified electrodes, fast diffusion, perylene diimide, pyrazolate ligand, multi-redox processes.*

**ABSTRACT:** Metal-organic frameworks (MOFs) featuring redox activity are highly appealing for electrocatalytic or charge accumulation applications. An important aspect in this field is the ability to address as many redox centers as possible in the material by an efficient diffusion of charges. Herein, we investigate for the first time the charge diffusion processes occurring upon two sequential one-electron reductions in a MOF thin film. Two pyrazolate-zinc(II) based metal-organic frameworks (MOFs) including highly electro-deficient perylene diimide (PDI) ligands were grown on conducting substrates, affording thin films with double n-type electrochromic properties as characterized by spectroelectrochemical analysis. In depth electrochemical and chronoabsorptiometric investigations were carried out to probe the charge diffusion in the MOF layers and highlighted significant differences in terms of diffusion kinetics and material stability, between the first and second successive reduction of the redox active PDI linkers. Our results show that MOFs based on multi-redox centers are more sensitive to encumbrance-related issues than their mono-redox analogues in the context of electrochemical applications, an observation that further underlines the fundamental aspect of pore dimensions toward efficient and fast ion diffusion.

## Introduction

Metal-Organic Frameworks (MOFs) featuring redox activity are of outmost interest for their potential applicability in resistive chemical sensing,<sup>1–3</sup> photovoltaics,<sup>4–6</sup> capacitors,<sup>7–10</sup> electrochromic switching<sup>11,12</sup> and electrocatalysis.<sup>13–17</sup> Hence, extensive efforts have been devoted to increase conductivity in MOFs.<sup>18–24</sup> However, as underlined by Morris *et al.*,<sup>25</sup> for the specific applications related to electrochemical systems, such as electrocatalysis or faradic charge accumulation, achieving high conductivities can arise via through-plane band-like transport,<sup>23</sup> is not a mandatory requirement to promote efficient electrochemical activity. In such systems, the limiting process will be ionic diffusion through the porous structure, and diffusion of the substrate and product during catalysis.<sup>26,27</sup> In that regard, conductivity is *partially* irrelevant for such applications, and the macroscopic diffusion of charge in these systems is often preferably considered. An important goal in this field is, hence, not necessarily to induce high conductivity but efficient overall diffusion of charges, both ionic and electronic.

These diffusive processes have been explored both theoretically and experimentally. The related studies, however, primarily focus on straightforward situations, where one type of redox center induces redox-activity by charge hopping, involving a single one-electron process (*e.g.*, oxidation of ferrocene, porphyrin or pyrene).<sup>27–31</sup> Indeed, while few reports in the literature address successive one-electron redox processes, there is a lack of in-depth investigation of the implications of such consecutive events on the diffusion of charges.<sup>12,12,16,30–33</sup> Shining light on the parameters that govern successive multi-redox events is crucial to improve the



**Scheme 1.** General synthesis of dual electrochromic Zn-MOF-modified electrodes.

comprehensive applicability of MOF for electrochemical applications mentioned above.

Classical electrochemical tools such as chronoamperometry might not be sufficient to distinguish two events occurring in a close range of potential. However, provided that the concerned redox centers are chromophores, which is often true in this field, the material is expected to present electrochromism (EC). This feature allows to monitor the redox events and the changes in absorbance that can be directly linked to the apparent diffusion of charge by chronoabsorptiometry, as demonstrated in several reports.<sup>34–36,30,15</sup> With this in mind, this approach might allow to distinguish, with

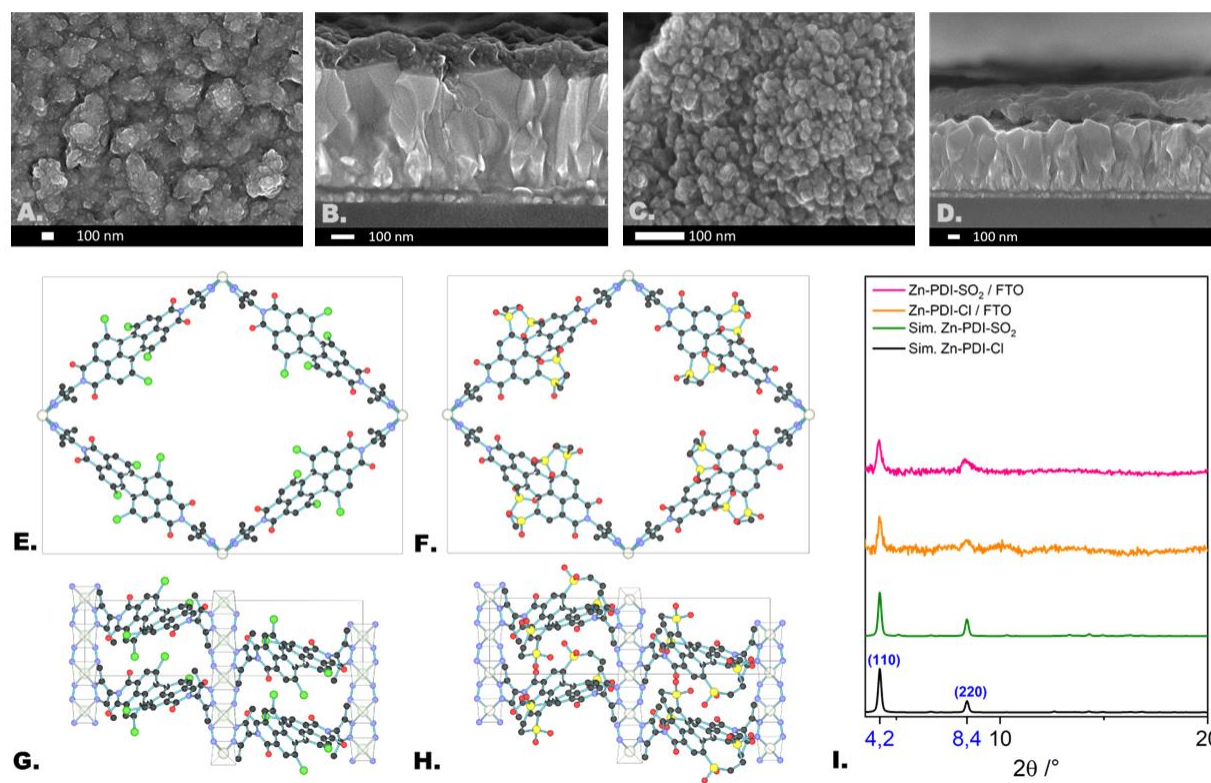


Figure 1. SEM images of the (A) top view and (B) side view of Zn-PDI-Cl on FTO electrodes, (C) top view and (D) side view of Zn-PDI-SO<sub>2</sub> on FTO electrodes. Computed structures of Zn-PDI-Cl viewed along (E) the c axis and (G) b axis and of Zn-PDI-SO<sub>2</sub> viewed along (F) the c axis and (H) b axis. (I) Experimental and simulated X-ray diffractograms for both materials.

satisfactory resolution, the diffusion processes occurring during successive redox events.

In this work, we provide a first case study of two successive one-electron processes, considered independently from one another, in a redox active MOF thin film. Electrochromism was used as a tool to probe the charge diffusion through two isostructural MOFs immobilized on transparent conductive electrodes, in which n-type redox activity is induced solely by highly electron deficient azolate perylene diimide linkers, with metal nodes used only as structural entities (**Scheme 1**). The non-participation of the metal nodes to the redox processes was desired to keep this case study as simple as possible. The chosen metal cation was Zn<sup>II</sup>, known for its redox-innocence on a broad electrochemical range and for forming rather stable networks in association with pyrazolate ligands.<sup>37</sup> Using a chronoabsorptometric approach we have independently determined the apparent diffusion coefficient for two successive reduction processes, by simultaneously monitoring the rate of formation and disappearance of neutral, mono-reduced and di-reduced species in MOF thin layers upon applied bias. The results revealed significant differences in the charge diffusion kinetics between the first and second successive reduction events within the same materials and allows us to propose correlations between the MOF film morphology, the pore channel dimensions and the diffusing counter ions with the charge diffusion ability and MOF film stability over repeated redox events.

## Results and discussion

### Thin films synthesis and characterization

We report herein the preparation of nanosized Zn-PDI-MOF thin-films with two previously published perylene diimide (PDI) pyrazolate ligands.<sup>38</sup> These films were grown *in situ* on fluoride tin oxide (FTO) substrates. The two PDI ligands are substituted in their four *bay* positions by either chlorine (PDI-Cl) or bridged ethyl-1,2-disulfone (PDI-SO<sub>2</sub>) groups (**Scheme 1**). These functionalizations enhance the electro-deficiency of PDI and allow to reach electrochromic behaviour at milder potentials than for their unfunctionalized homologue. It has indeed been previously demonstrated that these ligands can induce reversible and stable double *n-type* EC, via two successive one-electron reductions.<sup>38</sup>

The two different MOF-modified electrodes were synthesized by *in situ* direct growth by heating for 4h a solution of zinc nitrate and PDI ligands in presence of FTO-covered glass plate, as depicted in **Scheme 1** (see Supplementary Information for further details). The downward-oriented FTO face appeared covered by a homogeneous coloured thin layer. Scanning electron microscopy (SEM, see **Figure 1a-d** and **Figure S3b-d**) revealed the polycrystalline nature of the films, apparently composed of superimposed nanocrystallites, with a thickness of 100nm and 200nm for **Zn-PDI-Cl** and **Zn-PDI-SO<sub>2</sub>**, respectively.

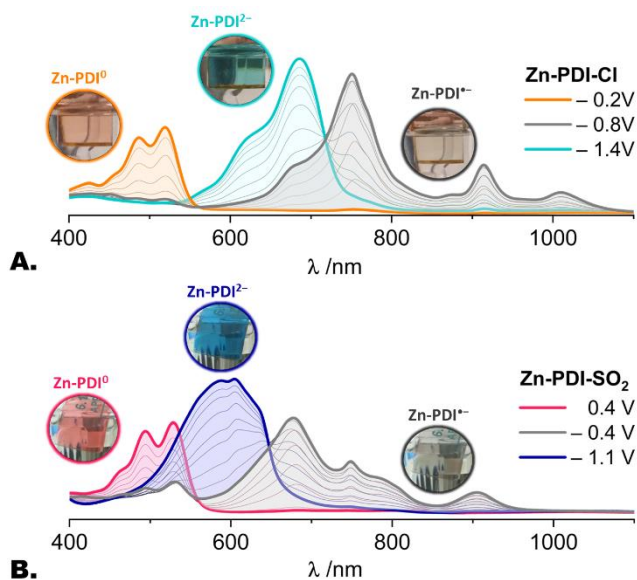


Figure 2. Spectroelectrochemical data: UV-Vis-NIR absorption spectra resulting of the application of increasingly cathodic potential steps on FTO electrodes modified with (A) Zn-PDI-Cl and (B) Zn-PDI-SO<sub>2</sub>. Each intermediate spectrum is associated with a specific potential step vs Ag/AgNO<sub>3</sub> (see Supplementary Information).

Zn-PDI-Cl and Zn-PDI-SO<sub>2</sub> are expected to be isostructural to a Zn<sup>2+</sup>-naphthalene diimide (NDI) pyrazolate MOF, reported by Dincă *et al.*<sup>33,39</sup> A distinctive feature of this structure is (-Zn-N-N-)∞ chains, in which Zn<sup>2+</sup> cations are in tetrahedral environment and spaced by the ligand, thus forming tetragonal channels.

To validate this hypothesis, we computed a structure derived from Co(dmdpb)<sup>40</sup> (dmdpb = 1,4-bis(3,5-dimethyl)di-pyrazol-4-ylbenzene). Additionally, the angle between two ligands around a given Zn chain, known to often deviate from the ideal 90°, was determined with the fitting routine MOF-FIT developed by Dincă *et al.*<sup>39</sup> The resulting angle was found to be 75° and the associated cell parameters were then used to optimize the geometry of the simulated structure (see Figures 1e-h and S5). The powder X-ray diffraction (PXRD) patterns of the resulting simulations matched well the experimental ones (see Figure 1i, S3 and S7). While the unit cell parameters, matching with the through-pore distances between two zinc centers, are large (*e.g.* *a* = 26.49 Å and *b* = 34.53 Å, see Supplementary Information), the actual free space for electrolyte to diffuse in is significantly smaller, due to the transversal orientation of the PDI cores. The diagonal distance through the channel, represented by the distance between the chlorine atoms of opposite ligands (see Figure S6a) is of *d*<sub>vdW(Cl-Cl)</sub> = 11 Å. Analogously, this distance shrinks to *d*<sub>vdW(H-H)</sub> = 8.8 Å, for Zn-PDI-SO<sub>2</sub>, underlining the higher encumbrance of the bridged sulfone groups (see Figure S6b). Prior to any chronoamperometric analysis, the n-electrochromic (EC) properties of the obtained films were studied by spectroelectrochemical measurements.

The recorded UV-vis-NIR spectra (Figure 2) are extremely similar to the corresponding spectra of the solvated ligands

(see Figure S8), showing an excellent conservation of the optical properties of the PDIs in the materials. Though, a perceptible variation does exist in the vibronic peaks' ratio of Zn-PDI-Cl and Zn-PDI-SO<sub>2</sub> (see Figure S8). For both closed-shell ground states PDI<sup>0</sup> and PDI<sup>2-</sup>, this ratio decreases slightly which is consistent with the presence of minor H-aggregation in the material.<sup>41,42</sup> Additionally, it has been shown that for naphthalene diimide (NDI) analogues, Coulomb coupling, inducing H-aggregation, between facing chromophores was possible at rather long distances of 6.8 Å.<sup>43</sup> The shortest inter-linker distance, corresponding to the *c* parameter, is about 7.2 Å in our Zn-PDI MOFs.

In addition, for Zn-PDI-SO<sub>2</sub>, the radical state PDI<sup>•-</sup> cannot be isolated without significant traces of the neutral state PDI<sup>0</sup>, observable between 450nm and 550nm. Whereas for Zn-PDI-Cl, apparent complete conversion of the ligands in each redox state can be readily achieved. This difference can be explained by a higher separation of the redox events for Zn-PDI-Cl than for Zn-PDI-SO<sub>2</sub>, possibly arising from a difference in the apparent diffusion of charges through each material. Following the characterisation of the electrochromic properties, the electrochemical response can allow to reach a first insight on charge diffusion inside these MOF layers.

#### Electrochemical analysis

A first investigation of the relative diffusive properties of the films was performed by cyclic voltammetry (CV) with increasing scan rates *v* = 10-1000mV/s (see Figure 3a and inset at 50mV/s). The aim was to probe the redox potentials in both materials and to have a first insight on differences between the first and second redox events in a given MOF film. Prior to any in-depth electrochemical (or spectroelectrochemical) analysis, the films were systematically activated by cyclic voltammetry, which also allowed to probe for the actual detection of the PDI electrochemical signature (see Figures S9 and S10).

The observation of only faradic current at low scan rate is consistent with charges diffusion by redox-hopping mechanism. At low scan rates (*v* = 10-100mV/s), both materials exhibit two distinguishable redox events, attributed to PDI reductions. However, increasing values of *v* highlights differences: *i)* Zn-PDI-Cl keeps well-distinguished redox events and exhibit lower separation Δ*E*<sub>p</sub> of the reduction and oxidation peaks potentials *E*<sub>pc</sub> and *E*<sub>pa</sub>, respectively, but *ii)* Zn-PDI-SO<sub>2</sub> quickly present merging redox events and an up to 6-fold higher peak separation (see Figure 3b and 3c). This difference of peak separation is consistent with a better charge diffusion in the less-hindered Zn-PDI-Cl, and might also partially result from a slower interfacial electron transfer rate between FTO and Zn-PDI-SO<sub>2</sub>. Similarly, observing that for Zn-PDI-Cl, Δ*E*<sub>p1</sub> is consistently lower than Δ*E*<sub>p2</sub> hints a difference between the first and second apparent charge diffusion.

When considering the electrochemical response of MOFs in the context of cyclic voltammetry, two regimes are theoretically distinguished, as notably discussed by Ott *et al.*<sup>26</sup>: *i)* a "fast" regime, giving a finite diffusional response, for which the diffusion of charges through the structure is fast enough

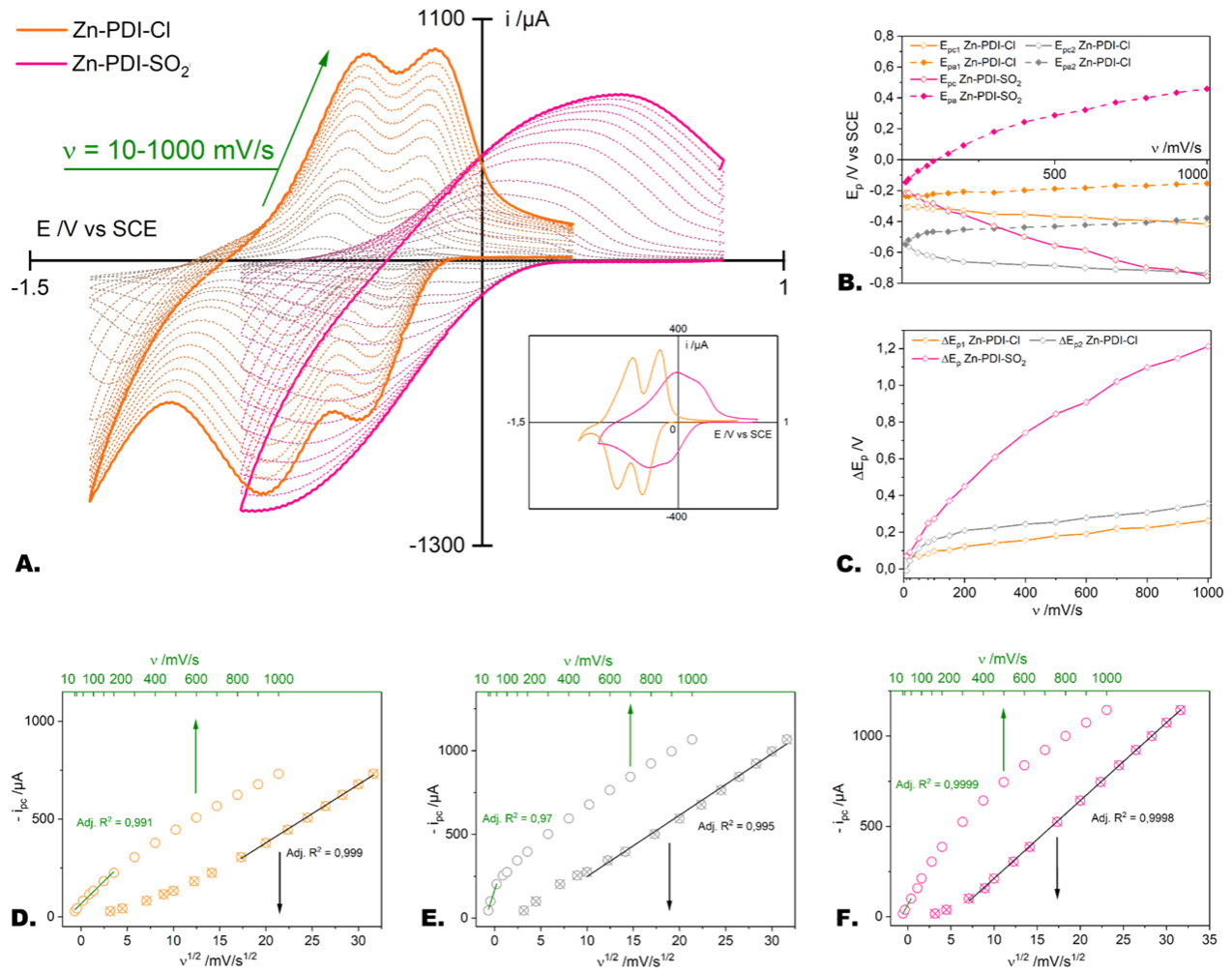


Figure 3. (A) Cyclic voltammograms for Zn-PDI-Cl (orange) and Zn-PDI-SO<sub>2</sub> (pink) at varying scan rate  $v = 10$ -1000 mV/s (inset: data at moderate scan rate  $v = 50$  mV/s), (B) redox peaks potentials  $E_p$  as a function of scan rate  $v$  and (C) relative difference  $\Delta E_p$  between the cathodic and anodic peaks potential  $E_{p,c}$  and  $E_{p,a}$ , respectively.  $i(v)$  and  $i(v^{1/2})$  plots for (D) first redox event peak current  $i_{p,c,1}$  and (E) second redox peak current  $i_{p,c,2}$  of Zn-PDI-Cl and (F) fused redox events peak current  $i_{p,c}$  of Zn-PDI-SO<sub>2</sub>.

compared to  $v$  to induce a diffusion layer of counter-ions thicker than the film and a linear response of  $i(v)$ , and ii) a “slow” regime, giving a semi-infinite diffusional response, for which the diffusion of charges through the structure is too slow compared to  $v$  and induces a diffusion layer of counter-ions thinner than the film and a linear response of  $i(v^{1/2})$ . Both of these regimes are distinguished by an adimensional parameter  $\lambda_e$ , first defined by Andrieux and Sav ant in 1980,<sup>44</sup> representing the ratio between the film thickness  $d_f$  and the diffusion layer thickness  $d_{diff}$ :

$$\lambda_e = \frac{d_f}{d_{diff}} = \frac{d_f}{\sqrt{\frac{D_{app}RT}{Fv}}} \quad (1)$$

Where  $D_{app}$  represents the apparent diffusion coefficient of charges,  $R$  the perfect gases constant,  $F$  the Faraday constant,  $T$  the temperature and  $v$  the scan rate. The fast regime is observed for  $\lambda_e \rightarrow 0$  and the slow regime for  $\lambda_e \rightarrow \infty$ . Hence, in theory, every MOF-modified electrode presents a shift of regime, characterized by a critical scan rate  $v_{critical}$

corresponding to the equalization of both  $d_f$  and  $d_{diff}$ . In reality, the vast majority of MOF-modified electrodes present a semi-infinite electrochemical response even at the lowest classically studied  $v$  (10 mV/s) and thus the aforementioned regime shift is not observed. This can be rationalized by the fact that the most common thickness  $d_f \approx 1 \mu\text{m}$  and apparent diffusion coefficients  $D_{app} \approx 10^{-10}$  to  $10^{-14} \text{cm}^2/\text{s}$  are conjointly too high and too low to induce a  $v_{critical}$  observable in the usual scope of the experiment (see **Table S2** and **Supplementary Information** for further details).<sup>14,15,28-31,45,46</sup>

Hence, the observation of this regime shift can suggest a high diffusion coefficient for the studied film. Here, as depicted in **Figure 3d-f** both materials present such a shift. Furthermore, since **Zn-PDI-Cl** electrochemical signature maintains a clear distinction between both first and second reductions, it is possible to determine  $v_{critical}$  for both first and second reductions. The change of linearity from  $i_p(v)$  to  $i_p(v^{1/2})$  occurs between  $v = 150$  mV/s and  $v = 300$  mV/s for the first reduction, whereas it occurs between  $v = 50$  mV/s

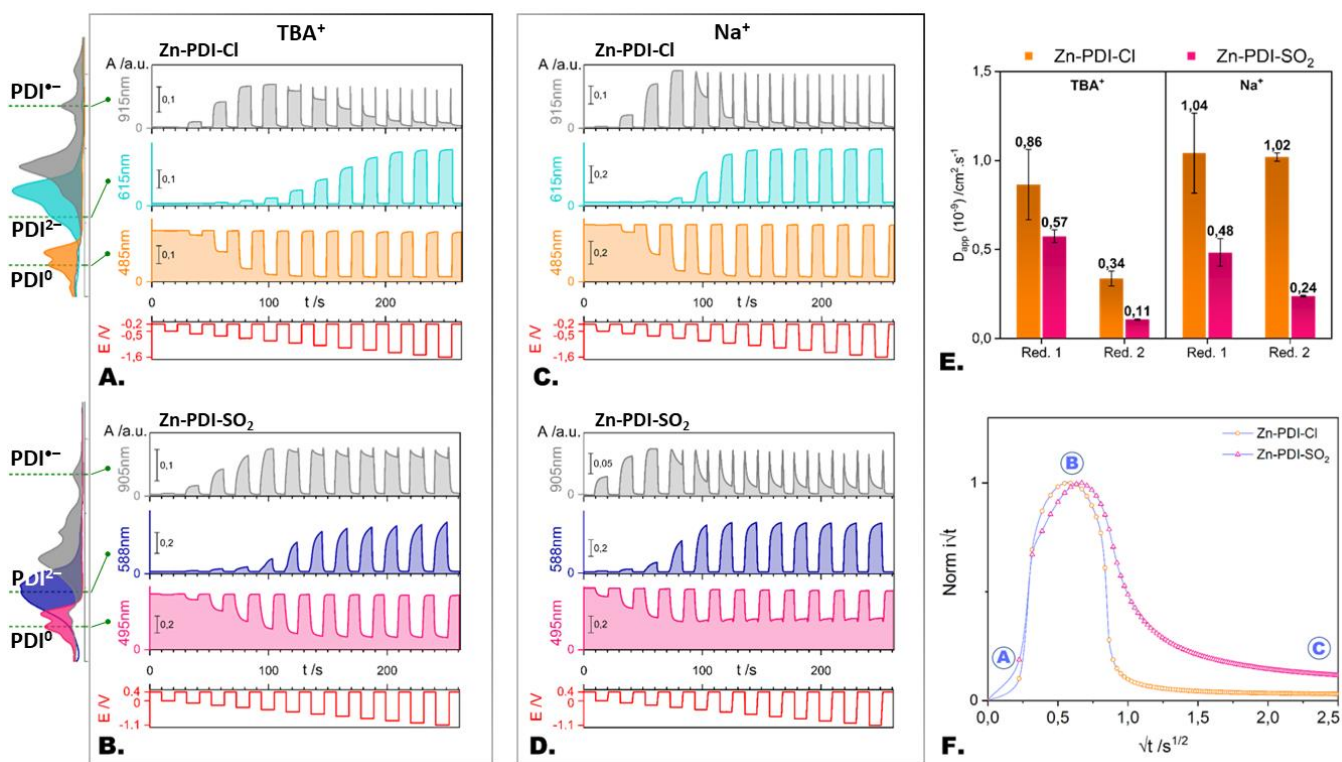


Figure 4. Chronoabsorptometric measurements, collected in TBA-based electrolyte (A) for Zn-PDI-Cl, (B) for Zn-PDI-SO<sub>2</sub> and collected in Na-based electrolyte (C) for Zn-PDI-Cl, (D) for Zn-PDI-SO<sub>2</sub> and (E) related apparent diffusion coefficient  $D_{app}$ . (F)  $i\sqrt{t}$  vs  $\sqrt{t}$  plots for Zn-PDI-Cl and Zn-PDI-SO<sub>2</sub> in Na<sup>+</sup>-based electrolyte.

and  $v = 100$  mV/s for the second reduction (see **Figure 3d-e**). This difference in  $v_{critical}$  suggests a significant difference between the kinetics of the first and second reduction events. Ott *et al.* recently demonstrated that TBA<sup>+</sup> counter ions do not induce strong enough ion-pairing with reduced arylene diimides to result in a noticeable difference in electrochemical response between the first and second reduction events.<sup>31</sup> Hence, this difference can result either from limitation in ion diffusivity or from electron diffusivity in the course the reduction process. On one hand, it is highly probable that both of these sources of variations impact the observed properties, as they are interacting in many ways. On the other hand, it is possible to postulate that the limited ion diffusion for the second reduction process is due to a locally lower diffusivity of TBA<sup>+</sup> in pores that already contain one TBA<sup>+</sup> for each PDI<sup>-</sup> generated by the first reduction. Hence, the second reduction of such a multi-redox system will always be slower, due to coulombic repulsions and steric hindrances, provided that the pores are not large enough to minimize such interactions.

Unfortunately, the CVs of **Zn-PDI-SO<sub>2</sub>** does not allow such a comparison since the two peaks quickly merge with the increase of  $v$ . Nonetheless, the merged peaks intensity  $i_p$  exhibit linearity with  $v^{1/2}$  starting at  $v = 50$  mV/s which tends to indicate that both first and second events are in the “slow” regime (semi-infinite diffusional response) at this scan rate (**Figure 3f**). Thus, the overall diffusion of charges in **Zn-PDI-SO<sub>2</sub>** appears again slower than in **Zn-PDI-Cl**, most likely due to the more hindered pore structure of the first compared to the latter. Finally, the lack of resolution of the electrochemical approach on these events legitimates

the use of chronoabsorptometry to probe for specific kinetics of both successive redox events.

#### Step-Chronoabsorptometry (SCA)

Whereas spectroelectrochemical measurements allowed to probe the redox species PDI<sup>0</sup>, PDI<sup>-</sup> and PDI<sup>2-</sup> in steady state, investigating the kinetics of the system requires a dynamic study. Thus, step-chronoabsorptometry (SCA) was performed. This method consists in monitoring the variation of charge and absorption at discrete wavelengths ( $\lambda(PDI^0)$ ,  $\lambda(PDI^-)$ ,  $\lambda(PDI^{2-})$ ) upon stepwise sweep ( $\Delta E$ ) from a starting potential ( $E_1$ ) to an end potential ( $E_2$ ). Each cathodic step was followed by an anodic switch to a fixed potential ( $E_{reset}$ ), at which the system’s neutrality is restored and every ligand is oxidized back to PDI<sup>0</sup>. For the sake of clarity, the chosen conditions are summed-up in **Table 1**.

Table 1. Parameters used for the acquisition of SCA data depicted in figure 4.

	Zn-PDI-Cl	Zn-PDI-SO <sub>2</sub>
$\lambda(PDI^0)$ /nm	485	495
$\lambda(PDI^-)$ /nm	915	905
$\lambda(PDI^{2-})$ /nm	615	588
$E_1$ /V <sup>[a]</sup>	-0.5	0
$E_2$ /V <sup>[a]</sup>	-1.6	-1.1
$\Delta E$ /V	-0.1	-0.1
$E_{reset}$ /V <sup>[a]</sup>	-0.2	0.4

[a] Potentials versus Ag/AgNO<sub>3</sub> reference electrode

The SCA plots (see **Figure S12**) depict the superimposed variations of charge and absorbance at every wavelength upon application of steps of potential for 10 seconds (bottom). The simultaneous variation of charge and absorbance confirms that the absorbance variations are indeed induced by charge injection in the material.

Further discussion will focus on the absorbance variations, and for sake of clarity, charge evolution will not be depicted on following plots (**Figure 4a-d**) and every cited or depicted potential will be *versus* Ag/AgNO<sub>3</sub> couple. For **Zn-PDI-Cl** (**Figure 4a-c**), the absorption at  $\lambda(\text{PDI}^0) = 485$  nm corresponding to the neutral PDI<sup>0</sup> quickly starts to decrease at  $E = -0.6$  V as the signal of the radical PDI<sup>•-</sup> appears at  $\lambda(\text{PDI}^{\bullet-}) = 915$  nm. This latter signal maxes out at  $E = -0.9$  V. At this potential, the slight increase in absorption at  $\lambda(\text{PDI}^{2-}) = 615$  nm can be partially attributed to the radical absorption (see **Figure S11**). At this threshold potential, the disappearance of PDI<sup>0</sup> reaches a plateau and further cathodic steps induce the formation of PDI<sup>2-</sup> by reduction of PDI<sup>•-</sup>. The plateau of absorbance of PDI<sup>2-</sup> is reached at  $E = -1.5$  V. One can notice that the plot of the absorbance at  $\lambda(\text{PDI}^{\bullet-})$  presents spikes of the same intensity as the aforementioned  $\lambda(\text{PDI}^{\bullet-})$  plateau. These spikes attest of the prior reduction of the PDI ligands in the material to PDI<sup>•-</sup> before their reduction to PDI<sup>2-</sup> takes place. This apparently obvious observation supports that the double electron transfer reaction  $\text{PDI}^0 + 2e^- \leftrightarrow \text{PDI}^{2-}$  is not occurring, as expected. Furthermore, this means that the curves of  $\lambda(\text{PDI}^0)$  and  $\lambda(\text{PDI}^{2-})$  contain direct information regarding the kinetics of the first and second redox events, respectively. As a general remark, the squareness of the waves attests for a complete and thus fast process.

In regard to the previous observations, **Zn-PDI-SO<sub>2</sub>** appears as a slower system. Whereas the absorbance seems to reach a decently low value at  $\lambda(\text{PDI}^0) = 495$  nm and a plateau at  $\lambda(\text{PDI}^{\bullet-}) = 905$  nm for  $E = -0.4$  V, the waves do clearly not present the square shape of the previous plot. In addition, spikes can only be observed at  $\lambda(\text{PDI}^{\bullet-})$  for the back oxidation, while the decrease of absorbance following the first reduction follows a weak slope. This observation tends to indicate that, while the system can decently get reduced to the first PDI<sup>•-</sup> state, 10 seconds steps are not long enough to allow **Zn-PDI-SO<sub>2</sub>** to be fully reduced to the PDI<sup>2-</sup> state, implying lower kinetics of conversion for the second redox event. This qualitative observation is consistent with the differences observed for **Zn-PDI-Cl** in the electrochemical study. In addition to qualitative information, quantitative data can be extracted from the chronoabsorptometric analysis, such as the coloration times  $t_c$  or the apparent charge diffusion coefficients  $D_{\text{app}}$ . The former underlines again the appearing slower diffusion of charges for the second event, as for instance  $t_c(\text{PDI}^0) = 0.18$  s and  $t_c(\text{PDI}^{2-}) = 0.71$  s, for **Zn-PDI-Cl** (see Supporting Information). The latter is accessible *via* a modified Cottrell equation, and will be discussed in details, as it represents the most meaningful information of this study.

Prior to this quantitative approach, it is relevant to incorporate additional variability in this study in order to gain insight on the origin of the appearing differences of kinetics

between the first and second redox events. To do so, a common way is to change the size and chemical nature of the diffusing species *i.e.*, here the cation of the supporting salt in the electrolyte. Based on the study of Wang *et al.*,<sup>47</sup> we chose Na<sup>+</sup> cations, representing the a decent balance between size and ion pairing with reduced arylene diimides. The resulting plots are depicted in **Figure 4c-d**.

The impact of this smaller cation on the rate of the systems is clearly visible and affects even the already fast **Zn-PDI-Cl** system, for which one can notice the enhanced squareness of the curves. Furthermore, the spectral signature of PDI<sup>2-</sup> can be detected at milder potential  $E = -0.8$  V, as the  $\lambda(\text{PDI}^{\bullet-})$  curve maxes out. The most noticeable effect can be observed on the  $\lambda(\text{PDI}^{2-})$  curve. The absorption is able to reach a plateau for potentials as low as  $E = -1.1$  V, which is 400 mV lower than with TBA<sup>+</sup> cations.

Similar effects can be observed for **Zn-PDI-SO<sub>2</sub>**. In addition, Na<sup>+</sup> cations allow for a more complete conversion of PDI<sup>•-</sup> in PDI<sup>2-</sup>, as depicted by the  $\lambda(\text{PDI}^{\bullet-})$  curve reaching a near zero absorbance value and the resulting appearance of previously unobservable spikes.

To get a quantitative appreciation of the fastness of the redox system, it is possible to extract apparent diffusion coefficients from the variation of absorbance by using the following modified Cottrell equation (see Supporting Information for more details):

$$\Delta A(\lambda) = \frac{2\Delta A_{\text{max}}(\lambda)\sqrt{D_{\text{app}}t}}{d_f\sqrt{\pi}} \quad (2)$$

Where  $\Delta A_{\text{max}}$  is the maximal variation of absorbance and  $d_f$  is the thickness of the film. The resulting diffusion coefficients (see **Figure 4e** and **Table S1**) land among the highest reported in the literature for MOF-modified electrodes (see **Table S2**).<sup>14,15,28-31,45,46</sup>

These diffusion coefficients are consistent with the previous observations and follow the tendencies: *i*)  $D_{\text{app}}(\text{Zn-PDI-Cl}) > D_{\text{app}}(\text{Zn-PDI-SO}_2)$  for a given reduction event and a given cation, *ii*)  $D_{\text{app},1} > D_{\text{app},2}$  for a given material and a given cation and *iii*)  $D_{\text{app}}(\text{Na}^+) \geq D_{\text{app}}(\text{TBA}^+)$  for a given material and a given reduction event. Noticeably, the change from TBA<sup>+</sup> to Na<sup>+</sup> does not seem to impact dramatically the first reduction, possibly due to the lack of coulombic repulsions and steric hindrances at the corresponding ion concentrations. Moreover, this change of cation allows for a reduction of the ratio  $D_{\text{app},1}/D_{\text{app},2}$  which is also consistent with an ionic diffusion control of the differences in kinetics between first and second reduction events.

In order to visualize the steps of the charge diffusion and partially distinguish between electronic and ionic diffusions, the model of Scholz<sup>48</sup> can be applied, as previously reported in the context of MOFs.<sup>27</sup> We hereinafter propose a critical discussion of this model regarding *i*) the applicability and relevance of this model for MOF multi-layered thin films in general, *ii*) the specific case of successive redox events in such materials.

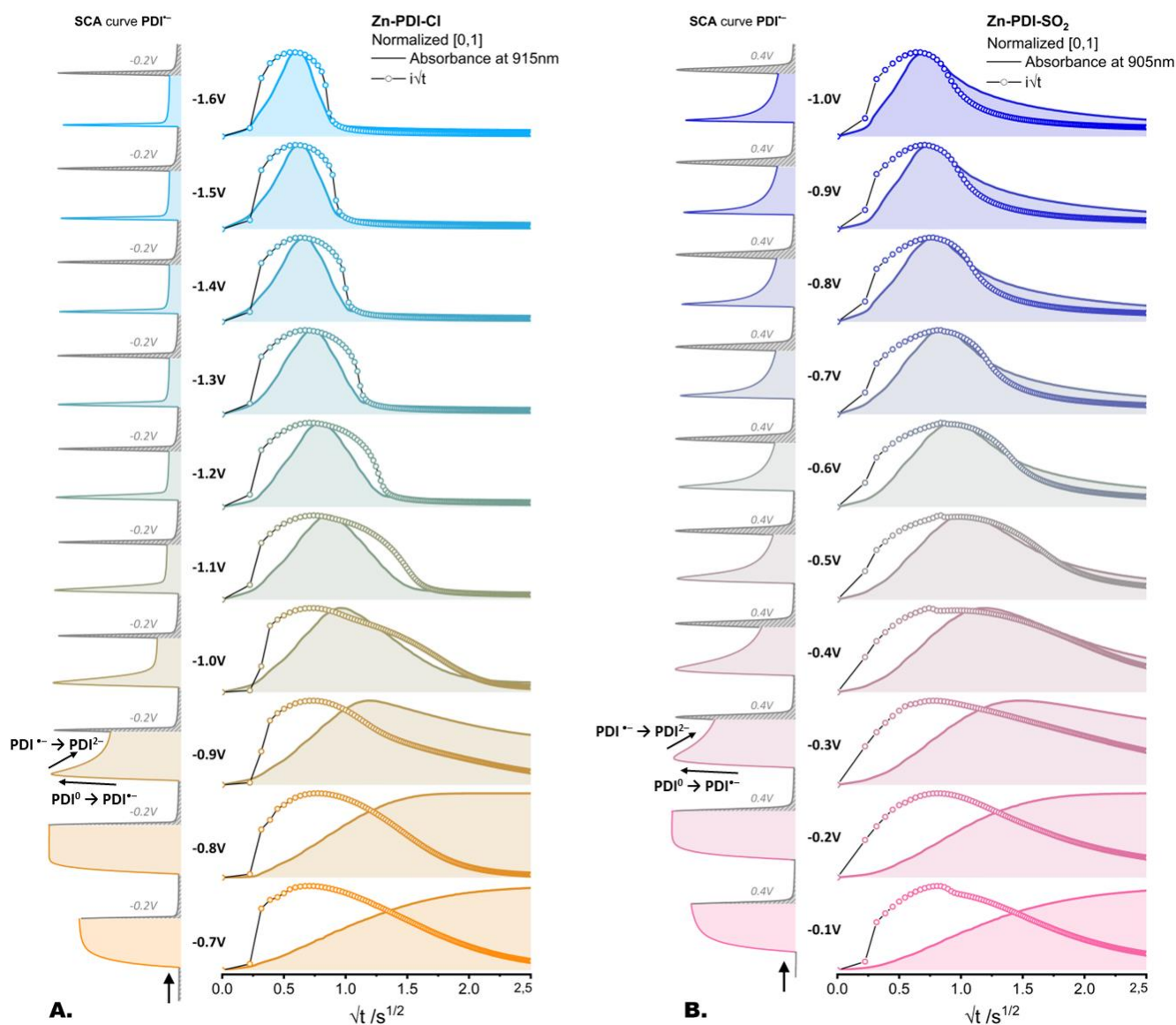


Figure 5: Normalized  $it^{1/2}$  vs.  $(t^{1/2})$  and  $A(\lambda(PDI^{\cdot-}))$  vs.  $(t^{1/2})$  curves for (A) Zn-PDI-Cl and (B) Zn-PDI-SO<sub>2</sub>, extracted from the SCA experiments, using Na<sup>+</sup> as a diffusing cation, as represented in **Figure 4c, d**. The left part of both figures reports the corresponding full SCA curve for PDI<sup>•-</sup>, as a reading aid marking the overall evolution of absorbance over the reported potential steps. The applied cathodic steps (V vs Ag/AgNO<sub>3</sub>) are depicted in black and the anodic, resetting, steps in grey

#### Model of Scholz: main feature

The most significant feature of this model is the plot of  $it^{1/2}$  vs.  $(t^{1/2})$ . To support further discussion, refer to **Figure 4f**, depicting  $it^{1/2}$  vs.  $(t^{1/2})$  curves for both materials, as extracted from the most cathodic step of the SCA experiments. Briefly, 3 main stages have been identified: the first stage (A) correspond to first electron jumps at the three-phase junction (crystal-electrode-solution) and is followed by pseudo-stage (A)→(B), corresponding to the propagation of the redox events from this junction. The process type (*i.e.* its directionality) is controlled by the fastest rate between electrons or counter-ions diffusions (**Figure 4f**). However, Morris *et al.* demonstrated experimentally that the ionic diffusion is always several orders of magnitude slower than the electronic diffusion, even for extremely wide pores (*e.g.*,

ferrocene-modified NU-1003, 47Å hexagonal pores) and for hopping-based electron diffusion.<sup>29</sup> Thus, the first step of the redox process is assimilated to a conversion of the redox centers along the faces of the crystal (*i.e.*, crystal-solution interface). Hence, pseudo-stage (A)→(B) is associated with ion diffusion from a quasi-semi-infinite medium, only limited by electron diffusion and related to the initial increase of the curve. The second stage (B) is reached when the faces are fully converted, which matches with the plot maximum. The subsequent decrease —pseudo-stage (B)→(C)— is linked to the diffusion of charges into the bulk of the crystal. This process is thus limited by the diffusion of counter-ions through the pores. The last stage (C) is reached when the redox active units in the crystal are almost completely converted.

## Model of Scholz: applicability

Directly apply this model to any MOF layer on an electrode can be appealing. However, Scholz model was established for a single micro-sized crystal on an electrode. The application of such a model, realized by Morris et al. in the aforementioned studies was brilliantly performed on single layers of well-dispersed micro-crystals, which allowed to effectively transpose this model into reality. While this application was essential to get access to general fundamental information on the behavior of MOFs upon electrochemical conversion, the present work aims to provide the community with simple methods, applicable to as many as possible multi-redox-active MOF thin films. Such films are generally composed of numerous layers of crystallites aggregates of various sizes, specifically when created by *in situ* growth, as it is the case for **Zn-PDI-Cl** and **Zn-PDI-SO<sub>2</sub>**. The issue with such materials, with regard to Scholz model, is that the described steps of conversion are mixed, as the multiplication and overlapping of crystallites of variable sizes should result similarly in the multiplication and overlapping of their conversion processes, starting at different times after the application of a potential step at the electrode. It is hence impossible to unmix these contributions and apply the mathematical model to obtain quantitative data.

Additionally, for multi-redox systems, successive redox events can add another layer of complexity to the conversion phenomenon, as parts of the material will in principle start their second reduction prior to the completion of the first reduction in other parts of the material (*e.g.*, typically surface *versus* bulk).

Nonetheless, the curve  $it^{1/2}$  vs.  $(t^{1/2})$  may still be relevant despite the fact that the well-established stages A, B and C are most probably overlapping, as it still allows to qualitatively highlight stages of conversion, since overlapping of curves shifted in time should mainly result in the broadening of the curves but not in the complete loss of their intrinsic structure, being an initial increase of the signal mainly related to surface diffusions and a final decrease mainly correlated to bulk diffusion.

We hence aim to have a first glance at the relevance of the  $it^{1/2}$  vs.  $(t^{1/2})$  curve in the context of multi-layered MOF presenting successive redox events. We propose to consider both the evolution of absorbance  $A$  and of  $it^{1/2}$  in the square root of time space, as represented in **Figure 5**, which superimpose, for the SCA experiments using  $\text{Na}^+$  as a diffusing counter ion, the normalized curves  $A(\lambda(\text{PDI}^{\cdot-}))$  vs.  $(t^{1/2})$  and  $it^{1/2}$  vs.  $(t^{1/2})$ . The absorbance of the radical  $\text{PDI}^{\cdot-}$  was chosen as it allows to get simultaneous insights over both redox events.

## Data description

It has to be stated that for diffusional models (*i.e.*, Scholz's or Cottrell's), the applied potential, inducing diffusion, is supposed to be non-limiting. Hence, this potential is generally chosen as sufficiently beyond the involved redox couple potential. If this condition is not met, the diffusion speed will appear to have a dependency on the applied potential,

until a plateau can be reached. This phenomenon is observed for the first redox event  $\text{PDI}^0 \rightarrow \text{PDI}^{\cdot-}$ , in **Figure 5a** step **-0.7V** vs step **-0.8V**, and in **Figure 5b** step **-0.1V** vs step **-0.2V**, for **Zn-PDI-Cl** and **Zn-PDI-SO<sub>2</sub>**, respectively. This results in an apparent contraction of the  $it^{1/2}$  and  $A(\lambda(\text{PDI}^{\cdot-}))$  curves toward shorter times and the reach of *extrema* in the time window of the potential steps.

As the applied potential is further shifted in the cathodic region, the absorbance of  $\text{PDI}^{\cdot-}$  starts decreasing again after the initial increase, as the produced radicals are consumed by the second redox event  $\text{PDI}^{\cdot-} \rightarrow \text{PDI}^{2-}$ . This phenomenon is accompanied by a noticeable distortion of the  $it^{1/2}$  curve, which now includes the contributions of both the first and second redox events. This new contribution further contracts and merge into the first one until the overall shapes of  $it^{1/2}$  and  $A$  curves does not present noticeable differences from one step to another (*i.e.*, three last steps of both figures 5a and 5b).

## General observations

Firstly, the overall conversion process seems faster for higher potentials, regardless of the number of redox events. This statement is very well exemplified when comparing the steps **-0.8V** and **-1.6V** of **Figure 5a**. For both steps, the system undergoes a complete conversion over the  $2.5 \text{ s}^{1/2}$  squared timescale, but the **-1.6V** step induces an extremely accelerated conversion for two redox events with respect to the mono-redox conversion induced by the **-0.8V** step. This observation is of critical importance as it highlights the impact of the choice of potential to probe for charge diffusion through Cottrell-derived methods. Indeed, variations of  $D_{app}$  with the applied potential is never (to the best of our knowledge) considered in studies on redox active MOFs. The general method adopted by the community is to consider redox events probed by cyclic voltammetry or differential pulse voltammetry and to choose a potential located at proximity of the end of the considered event's peak. Thermodynamically, this method is justified and does allow a complete conversion of the film. But it has been demonstrated by Genies *et al.* for polypyrrole films that the influence of potential on charge diffusion could be non-negligible,<sup>49</sup> partly as it may impact the structure of the material and thus the charge migration, over a great range of potential located after the considered redox couple potential. On one hand, the extend of this effect is likely attributed to the flexibility of a polymeric film, and should hence be of greatly reduced impact for MOFs. On the other hand, verifying this assertion for each MOF appears to be relevant as we observe such an impact of potential in **Figure 5**. For the present situation, the three last steps, for which the kinetic features present negligible variations, were chosen for the determination of an averaged  $D_{app}$ . Finally, this observation underlines how the chronoabsorptometric approach is relevant for multi-redox systems as it allows to study both events at the same high potential, whereas a purely chrono-coulometric approach would not allow such a study, and may expose to potential-related issues when considering charge diffusion.

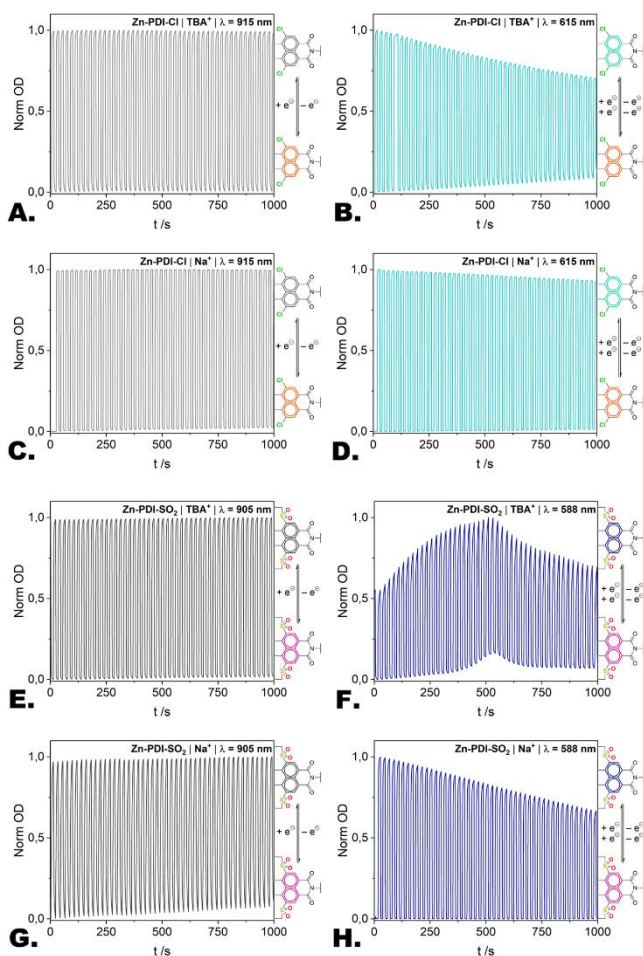


Figure 6. Stability of the Zn-PDI MOFs by monitoring of absorbance during cycling potential steps of 10s. Data for Zn-PDI-Cl in TBA-based electrolyte while cycling between (A) PDI<sup>0</sup> and PDI<sup>-</sup>, (B) PDI<sup>-</sup> and PDI<sup>2-</sup> and in Na-based electrolyte while cycling between (C) PDI<sup>0</sup> and PDI<sup>-</sup>, (D) PDI<sup>-</sup> and PDI<sup>2-</sup>. Data for Zn-PDI-SO<sub>2</sub> in TBA-based electrolyte while cycling between (E) PDI<sup>0</sup> and PDI<sup>-</sup>, (F) PDI<sup>-</sup> and PDI<sup>2-</sup> and in Na-based electrolyte while cycling between (G) PDI<sup>0</sup> and PDI<sup>-</sup>, (H) PDI<sup>-</sup> and PDI<sup>2-</sup>.

Interestingly, for the higher potential values, what is interpreted as the part mainly related to ionic diffusion of the  $it^{1/2}$  curves (located after the maximum —pseudo stage B→C of the idealized Scholz model—) appears in reality to correlate mainly to the second reduction event, as their maxima superimpose with the ones of  $A(\lambda(\text{PDI}^{\cdot-}))$ , the latter being the point at which the materials' first redox conversion is almost complete. This observation highlights the fact that the existing differences between the rates of the successive redox events seems to be the determining factor in the overall diffusional behavior and thus the shape of the  $it^{1/2}$  curves. To dive into the details of the implications of these data, the focus further is set on the last potential step of each set of data (*i.e.* -1.6V and -1.0V for Zn-PDI-Cl and Zn-PDI-SO<sub>2</sub>, respectively).

### Observations at high potential — Last step

The two last steps of both sets of data (*i.e.* -1.6V and -1.0V steps of figure 5a and 5b, respectively) act as relevant examples of general cases.

Firstly, one can note that as the maxima of the  $it^{1/2}$  and  $A(\lambda(\text{PDI}^{\cdot-}))$  curves match, the first pseudo-stage (A)→(B) mainly includes contributions from the first redox event, surface and bulk.

Secondly, and given by the previously established immense differences in the rates of surface *versus* bulk diffusion, this pseudo-stage (A)→(B) must also include some part of the surface diffusion from the second conversion. The second part of the  $it^{1/2}$  curve, namely pseudo-stage (B)→(C), is hence mainly related to the bulk diffusion of the second conversion reaction.

Lastly, the overall process occurs on very small timescales. Stage (C) is reached within  $t_c = 1$ s and  $t_c = 6.25$ s for Zn-PDI-Cl and for Zn-PDI-SO<sub>2</sub>, respectively. Moreover, the shape of the  $it^{1/2}(t^{1/2})$  curves are quite symmetrical compared to what was reported for Scholz ideal model<sup>48</sup> and by Morris *et al.* for real systems.<sup>27,29</sup> Whereas it is impossible to distinguish between the contributions of surface and bulk when considering both redox event, the symmetry of the  $it^{1/2}(t^{1/2})$  curve is also quite high for the lowest potential steps, for which only the first redox event occurs. This means that the contributions of surface and bulk diffusions, *i.e.*, Scholz ideal pseudo stage (A)→(B) and (B)→(C), respectively, extend over comparable times durations. These observations correlate with the overall fast conversion observed with every analytical method in this work. We rationalize this phenomenon in the following paragraph.

### General remarks

When considering a redox-hopping based MOF-modified electrode, one goal is obviously to reach stage (C) as fast as possible. To do so, one can shorten stage (B) by increasing ion diffusion rate, using wide pores and small, moderately-pairing electrolyte (*e.g.* Na<sup>+</sup> in our case). It is also possible to shorten stage (A) by using redox centers having high self-exchange rate constants as demonstrated by Morris *et al.* with NU-1000 modified with metallocenes based on Fe, Ru and Os.<sup>27</sup> However, one needs to take into account that: *i)* ion diffusion is always slower than electron diffusion and, *ii)* ion diffusion accounts for the main part of the overall conversion since the main part of the redox centers is located in the bulk of the crystal. These observations suggest that reducing the crystal size and thus increasing the surface to volume ratio will not only maximize the participation of stage (A), based on fast electronic diffusion, but also increase the overall rate of ionic diffusion by extending the crystal-electrolyte interface area though which ions can enter the bulk. Additionally, bulk ionic diffusion has been demonstrated as being the main source for existing differences between successive redox events, it is hence likely that reducing its participation to the overall charge diffusion would reduce such differences. One can also notice that the crystal sizes of the studied materials, whilst dispersed, seem superior for Zn-PDI-Cl than for Zn-PDI-SO<sub>2</sub> films (see Figure 1a, c and Figure S3a, c). This observation tends to

indicate that the participation of surface diffusion to the overall process could be higher for **Zn-PDI-SO<sub>2</sub>** than for **Zn-PDI-Cl**. This may therefore suggest that the aforementioned effects are ever-so-slightly underestimated in the present work, which does support the conclusions.

The present general remarks hold especially true for materials relying on redox-hopping promoted charge diffusion and is thus of particular relevance for related applications, such as electrocatalysis and faradic charge accumulation.

### Stability

Finally, the stability of **Zn-PDI-Cl** and **Zn-PDI-SO<sub>2</sub>** toward redox cycles was probed (see **Figure 6**), with cycles of alternating potentials targeting either the first redox event or both redox events. Different parameters can be considered regarding the materials stability, being: *i*) hindrance of the structure, *ii*) nature of the diffusing cations and *iii*) targeted reduced specie *i.e.*, PDI<sup>•-</sup> or PDI<sup>2-</sup>. As evidenced by *c.a.* 100% retention of the maximal optical density over 100 cycles, both films present excellent electrochemical stability when cycling between PDI<sup>0</sup> and PDI<sup>•-</sup> states and regardless of the diffusing cation (**Figure 6a,c,e,g**). However, the film cyclability drops when considering further reduction to the PDI<sup>2-</sup> state (**Figure 6b,d,f,h**). This again underlines differences between first and second redox events. As discussed previously, a subsequent reduction forces a second equivalent of counter-cations inside the porous structure. This constrained diffusion seems to strongly impact the materials integrity over time. It is probable that the higher energetic environment generated by inter-ion repulsions, as well as the presence of uncompensated injected charges, can favor degradation reactions at the weakest bonds of the materials, *ergo*, the coordination bonds. The repulsion-based nature of this degradation phenomenon is evidenced by stability trends comparable to those of diffusion coefficients. Furthermore, a similar trend has recently been demonstrated by Bessinger *et al.* with a series of COFs of different pore size, showing that more constrained environments lead to decreased stability upon electrochemical conversions.<sup>50</sup> It is also worth noticing that this limitation is almost overcome by using Na<sup>+</sup>-based electrolyte for **Zn-PDI-Cl**, implying that, even if a second redox event seems to be slower and induce instability, a rational choice of diffusing species can help to drastically reduce this effect.

### Conclusion

In summary, two nanosized-MOF modified electrodes were elaborated by *in situ* growth on FTO glass. These thin layers were formed by the self-assembly of Zn<sup>2+</sup> cations and electron deficient PDI-pyrazolate ligands, the latter acting as redox centers for the propagation and accumulation of electrons through the materials. The resulting MOF films exhibit double *n-type* electrochromism, a property that was exploited to assess the existence and extend of differences between multiple successive redox events, during rather fast charge diffusion. We have shown that chronoabsorptometric approach can be applied to identify and probe two distinct apparent diffusion coefficients for successive one-electron events. It is well-established that charge diffusion

efficiency is notably dependent on the ability of the counter ions to reach the redox centers within the material. We demonstrate here that a corollary effect is that further redox events in a series will be increasingly more difficult for each additional charge injected as the material pores will be filled with additional counter-ions, leaving less room for new ones to diffuse in. This effect has been illustrated with a lower  $D_{app}$  for the second reduction of Zn-PDI-Cl and Zn-PDI-SO<sub>2</sub> as compared to the first one. Also, this increased pore crowding over additional redox events tends to lower the MOF stability toward repeated redox cycling. Both stability and apparent rate of charge diffusion can be increased by using an electrolyte based on smaller (and poorly pairing) counter ions. In our case, Na<sup>+</sup> ions showed particularly pronounced effects for the second reduction event, underlining the profound ionic-based limitation of charge diffusion in redox-active MOFs based on redox hopping.

Finally,  $it^{1/2}$  vs.  $(t^{1/2})$ , derived from the Scholz model, and  $A(\lambda(PDI^{•-}))$  vs.  $(t^{1/2})$  curves were conjointly considered to get a detailed insight of the conversion process for multiple cathodic potential steps. Based on this set of data, we tried to provide the community with a critical discussion and to highlight the relevance of the chronoabsorptometric approach for probing multiple successive redox events in MOFs.

### ASSOCIATED CONTENT

(Word Style "TE\_Supporting\_Information"). **Supporting Information.** A brief statement in nonsentence format listing the contents of material supplied as Supporting Information should be included, ending with "This material is available free of charge via the Internet at <http://pubs.acs.org>." For instructions on what should be included in the Supporting Information as well as how to prepare this material for publication, refer to the journal's Instructions for Authors.

### AUTHOR INFORMATION

#### Corresponding Authors

Vincent Monnier - Nantes Université, CNRS, CEISAM, UMR 6230, F-44000 Nantes, France.  
[vincent.monnier@univ-nantes.fr](mailto:vincent.monnier@univ-nantes.fr)

Stéphane Diring - Nantes Université, CNRS, CEISAM, UMR 6230, F-44000 Nantes, France.  
[stephane.diring@univ-nantes.fr](mailto:stephane.diring@univ-nantes.fr)

#### Author Contributions

The manuscript was written through contributions of all authors. / All authors have given approval to the final version of the manuscript. /

#### Funding Sources

This work is funded by the ANR PhotoMOF project, Grant ANR-18-CE05-0008-01

#### Notes

Any additional relevant notes should be placed here.

### ACKNOWLEDGMENT

S.D. is grateful for financial support from ANR PhotoMOF project, Grant ANR-18-CE05-0008-01. We acknowledge Dr.

Thomas Devic and Dr. Fabrice Salles for fruitful discussion and help regarding structure modelling.

## REFERENCES

- (1) Campbell, M. G.; Liu, S. F.; Swager, T. M.; Dincă, M. Chemiresistive Sensor Arrays from Conductive 2D Metal–Organic Frameworks. *J. Am. Chem. Soc.* **2015**, *137* (43), 13780–13783. <https://doi.org/10.1021/jacs.5b09600>.
- (2) Smith, M. K.; Jensen, K. E.; Pivak, P. A.; Mirica, K. A. Direct Self-Assembly of Conductive Nanorods of Metal–Organic Frameworks into Chemiresistive Devices on Shrinkable Polymer Films. *Chem. Mater.* **2016**, *28* (15), 5264–5268. <https://doi.org/10.1021/acs.chemmater.6b02528>.
- (3) Kung, C.-W.; Platero-Prats, A. E.; Drout, R. J.; Kang, J.; Wang, T. C.; Audu, C. O.; Hersam, M. C.; Chapman, K. W.; Farha, O. K.; Hupp, J. T. Inorganic “Conductive Glass” Approach to Rendering Mesoporous Metal–Organic Frameworks Electronically Conductive and Chemically Responsive. *ACS Appl. Mater. Interfaces* **2018**, *10* (36), 30532–30540. <https://doi.org/10.1021/acsami.8b08270>.
- (4) Foster, M. E.; Azoulay, J. D.; Wong, B. M.; Allendorf, M. D. Novel Metal–Organic Framework Linkers for Light Harvesting Applications. *Chem. Sci.* **2014**, *5* (5), 2081–2090. <https://doi.org/10.1039/C4SC00333K>.
- (5) Lee, D. Y.; Shinde, D. V.; Yoon, S. J.; Cho, K. N.; Lee, W.; Shrestha, N. K.; Han, S.-H. Cu-Based Metal–Organic Frameworks for Photovoltaic Application. *J. Phys. Chem. C* **2014**, *118* (30), 16328–16334. <https://doi.org/10.1021/jp4079663>.
- (6) Kaur, R.; Kim, K.-H.; Paul, A. K.; Deep, A. Recent Advances in the Photovoltaic Applications of Coordination Polymers and Metal Organic Frameworks. *J. Mater. Chem. A* **2016**, *4* (11), 3991–4002. <https://doi.org/10.1039/C5TA09668E>.
- (7) Feng, D.; Lei, T.; Lukatskaya, M. R.; Park, J.; Huang, Z.; Lee, M.; Shaw, L.; Chen, S.; Yakovenko, A. A.; Kulkarni, A.; Xiao, J.; Fredrickson, K.; Tok, J. B.; Zou, X.; Cui, Y.; Bao, Z. Robust and Conductive Two-Dimensional Metal–organic Frameworks with Exceptionally High Volumetric and Areal Capacitance. *Nat. Energy* **2018**, *3* (1), 30–36. <https://doi.org/10.1038/s41560-017-0044-5>.
- (8) Li, W.-H.; Ding, K.; Tian, H.-R.; Yao, M.-S.; Nath, B.; Deng, W.-H.; Wang, Y.; Xu, G. Conductive Metal–Organic Framework Nanowire Array Electrodes for High-Performance Solid-State Supercapacitors. *Adv. Funct. Mater.* **2017**, *27* (27), 1702067. <https://doi.org/10.1002/adfm.201702067>.
- (9) Sheberla, D.; Bachman, J. C.; Elias, J. S.; Sun, C.-J.; Shao-Horn, Y.; Dincă, M. Conductive MOF Electrodes for Stable Supercapacitors with High Areal Capacitance. *Nature Mater* **2017**, *16* (2), 220–224. <https://doi.org/10.1038/nmat4766>.
- (10) Wang, L.; Han, Y.; Feng, X.; Zhou, J.; Qi, P.; Wang, B. Metal–Organic Frameworks for Energy Storage: Batteries and Supercapacitors. *Coordination Chemistry Reviews* **2016**, *307*, 361–381. <https://doi.org/10.1016/j.ccr.2015.09.002>.
- (11) Kung, C.-W.; Wang, T. C.; Mondloch, J. E.; Fairen-Jimenez, D.; Gardner, D. M.; Bury, W.; Klingsporn, J. M.; Barnes, J. C.; Van Duyne, R.; Stoddart, J. F.; Wasielewski, M. R.; Farha, O. K.; Hupp, J. T. Metal–Organic Framework Thin Films Composed of Free-Standing Acicular Nanorods Exhibiting Reversible Electrochromism. *Chem. Mater.* **2013**, *25* (24), 5012–5017. <https://doi.org/10.1021/cm403726v>.
- (12) AlKaabi, K.; Wade, C. R.; Dincă, M. Transparent-to-Dark Electrochromic Behavior in Naphthalene-Diimide-Based Mesoporous MOF-74 Analogs. *Chem* **2016**, *1* (2), 264–272. <https://doi.org/10.1016/j.chempr.2016.06.013>.
- (13) Downes, C. A.; Marinescu, S. C. Electrocatalytic Metal–Organic Frameworks for Energy Applications. *ChemSusChem* **2017**, *10* (22), 4374–4392. <https://doi.org/10.1002/cssc.201701420>.
- (14) Lin, S.; Pineda-Galvan, Y.; Maza, W. A.; Epley, C. C.; Zhu, J.; Kessinger, M. C.; Pushkar, Y.; Morris, A. J. Electrochemical Water Oxidation by a Catalyst-Modified Metal–Organic Framework Thin Film. *ChemSusChem* **2017**, *10* (3), 514–522. <https://doi.org/10.1002/cssc.201601181>.
- (15) Roy, S.; Huang, Z.; Bhunia, A.; Castner, A.; Gupta, A. K.; Zou, X.; Ott, S. Electrocatalytic Hydrogen Evolution from a Cobaloxime-Based Metal–Organic Framework Thin Film. *J. Am. Chem. Soc.* **2019**, *141* (40), 15942–15950. <https://doi.org/10.1021/jacs.9b07084>.
- (16) Castner, A. T.; Johnson, B. A.; Cohen, S. M.; Ott, S. Mimicking the Electron Transport Chain and Active Site of [FeFe] Hydrogenases in One Metal–Organic Framework: Factors That Influence Charge Transport. *J. Am. Chem. Soc.* **2021**, *143* (21), 7991–7999. <https://doi.org/10.1021/jacs.1c01361>.
- (17) McCarthy, B. D.; Beiler, A. M.; Johnson, B. A.; Liseev, T.; Castner, A. T.; Ott, S. Analysis of Electrocatalytic Metal–Organic Frameworks. *Coordination Chemistry Reviews* **2020**, *406*, 213137. <https://doi.org/10.1016/j.ccr.2019.213137>.
- (18) Kornienko, N.; Zhao, Y.; Kley, C. S.; Zhu, C.; Kim, D.; Lin, S.; Chang, C. J.; Yaghi, O. M.; Yang, P. Metal–Organic Frameworks for Electrocatalytic Reduction of Carbon Dioxide. *J. Am. Chem. Soc.* **2015**, *137* (44), 14129–14135. <https://doi.org/10.1021/jacs.5b08212>.
- (19) D’Alessandro, D. M. Exploiting Redox Activity in Metal–Organic Frameworks: Concepts, Trends and Perspectives. *Chem. Commun.* **2016**, *52* (58), 8957–8971. <https://doi.org/10.1039/C6CC00805D>.
- (20) Leong, C. F.; Usov, P. M.; D’Alessandro, D. M. Intrinsically Conducting Metal–Organic Frameworks. *MRS Bull.* **2016**, *41* (11), 858–864. <https://doi.org/10.1557/mrs.2016.241>.
- (21) Bhardwaj, S. K.; Bhardwaj, N.; Kaur, R.; Mehta, J.; Sharma, A. L.; Kim, K.-H.; Deep, A. An Overview of Different Strategies to Introduce Conductivity in Metal–Organic Frameworks and Miscellaneous Applications Thereof. *J. Mater. Chem. A* **2018**, *6* (31), 14992–15009. <https://doi.org/10.1039/C8TA04220A>.
- (22) Kung, C.-W.; Han, P.-C.; Chuang, C.-H.; Wu, K. C.-W. Electronically Conductive Metal–Organic Framework-Based Materials. *APL Materials* **2019**, *7* (11), 110902. <https://doi.org/10.1063/1.5125487>.
- (23) Xie, L. S.; Skorupskii, G.; Dincă, M. Electrically Conductive Metal–Organic Frameworks. *Chem. Rev.* **2020**, *120* (16), 8536–8580. <https://doi.org/10.1021/acs.chemrev.9b00766>.
- (24) Johnson, E. M.; Ilic, S.; Morris, A. J. Design Strategies for Enhanced Conductivity in Metal–Organic Frameworks. *ACS Cent. Sci.* **2021**, *7* (3), 445–453. <https://doi.org/10.1021/acscentsci.1c00047>.
- (25) Lin, S.; Usov, P. M.; Morris, A. J. The Role of Redox Hopping in Metal–Organic Framework Electrocatalysis. *Chem. Commun.* **2018**, *54* (51), 6965–6974. <https://doi.org/10.1039/C8CC01664J>.
- (26) Johnson, B. A.; Beiler, A. M.; McCarthy, B. D.; Ott, S. Transport Phenomena: Challenges and Opportunities for Molecular Catalysis in Metal–Organic Frameworks. *J. Am. Chem. Soc.* **2020**, *142* (28), 11941–11956. <https://doi.org/10.1021/jacs.0c02899>.
- (27) Celis-Salazar, P. J.; Cai, M.; Cucinell, C. A.; Ahrenholtz, S. R.; Epley, C. C.; Usov, P. M.; Morris, A. J. Independent Quantification of Electron and Ion Diffusion in Metallocene-Doped

- Metal–Organic Frameworks Thin Films. *J. Am. Chem. Soc.* **2019**, *141* (30), 11947–11953. <https://doi.org/10.1021/jacs.9b03609>.
- (28) Goswami, S.; Hod, I.; Duan, J. D.; Kung, C.-W.; Rimoldi, M.; Malliakas, C. D.; Palmer, R. H.; Farha, O. K.; Hupp, J. T. Anisotropic Redox Conductivity within a Metal–Organic Framework Material. *J. Am. Chem. Soc.* **2019**, *141* (44), 17696–17702. <https://doi.org/10.1021/jacs.9b07658>.
- (29) Cai, M.; Loague, Q.; Morris, A. J. Design Rules for Efficient Charge Transfer in Metal–Organic Framework Films: The Pore Size Effect. *J. Phys. Chem. Lett.* **2020**, *11* (3), 702–709. <https://doi.org/10.1021/acs.jpcllett.9b03285>.
- (30) Ahrenholtz, S. R.; Epley, C. C.; Morris, A. J. Solvothermal Preparation of an Electrocatalytic Metalloporphyrin MOF Thin Film and Its Redox Hopping Charge-Transfer Mechanism. *J. Am. Chem. Soc.* **2014**, *136* (6), 2464–2472. <https://doi.org/10.1021/ja410684q>.
- (31) Castner, A. T.; Su, H.; Svensson Grape, E.; Inge, A. K.; Johnson, B. A.; Ahlquist, M. S. G.; Ott, S. Microscopic Insights into Cation-Coupled Electron Hopping Transport in a Metal–Organic Framework. *J. Am. Chem. Soc.* **2022**, *144* (13), 5910–5920. <https://doi.org/10.1021/jacs.1c13377>.
- (32) Xie, Y.-X.; Zhao, W.-N.; Li, G.-C.; Liu, P.-F.; Han, L. A Naphthalenediimide-Based Metal–Organic Framework and Thin Film Exhibiting Photochromic and Electrochromic Properties. *Inorg. Chem.* **2016**, *55* (2), 549–551. <https://doi.org/10.1021/acs.inorgchem.5b02480>.
- (33) Wade, C. R.; Li, M.; Dincă, M. Facile Deposition of Multicolored Electrochromic Metal–Organic Framework Thin Films. *Angew. Chem. Int. Ed.* **2013**, *52* (50), 13377–13381. <https://doi.org/10.1002/anie.201306162>.
- (34) Strojek, J. W.; Kuwana, T.; Feldberg, S. W. Spectrochemical-Electrochemical Evaluation of Kinetics Using Optically Transparent Electrodes. *J. Am. Chem. Soc.* **1968**, *90* (5), 1353–1355. <https://doi.org/10.1021/ja01007a045>.
- (35) Winograd, N.; Blount, H. N.; Kuwana, T. Spectroelectrochemical Measurement of Chemical Reaction Rates. First-Order Catalytic Processes. *J. Phys. Chem.* **1969**, *73* (10), 3456–3462. <https://doi.org/10.1021/j100844a054>.
- (36) Yagi, M.; Sato, T. Temperature-Controlled Charge Transfer Mechanism in a Polymer Film Incorporating a Redox Molecule As Studied by Potential-Step Chronocoulometry. *J. Phys. Chem. B* **2003**, *107* (21), 4975–4981. <https://doi.org/10.1021/jp026859f>.
- (37) Pettinari, C.; Tăbăcaru, A.; Galli, S. Coordination Polymers and Metal–Organic Frameworks Based on Poly(Pyrazole)-Containing Ligands. *Coordination Chemistry Reviews* **2016**, *307*, 1–31. <https://doi.org/10.1016/j.ccr.2015.08.005>.
- (38) Monnier, V.; Odobel, F.; Diring, S. New Sulfonated Perylene Diimide Pyrazolate Ligands: A Simple Route toward n-Type Redox-Active Hybrid Materials. *Chem. Commun.* **2022**, *58* (67), 9429–9432. <https://doi.org/10.1039/D2CC02427F>.
- (39) Wade, C. R.; Corrales-Sanchez, T.; Narayan, T. C.; Dincă, M. Postsynthetic Tuning of Hydrophilicity in Pyrazolate MOFs to Modulate Water Adsorption Properties. *Energy Environ. Sci.* **2013**, *6* (7), 2172. <https://doi.org/10.1039/c3ee40876k>.
- (40) Tonigold, M.; Lu, Y.; Mavrandonakis, A.; Puls, A.; Staudt, R.; Möllmer, J.; Sauer, J.; Volkmer, D. Pyrazolate-Based Cobalt(II)-Containing Metal–Organic Frameworks in Heterogeneous Catalytic Oxidation Reactions: Elucidating the Role of Entatic States for Biomimetic Oxidation Processes. *Chem. Eur. J.* **2011**, *17* (31), 8671–8695. <https://doi.org/10.1002/chem.201003173>.
- (41) Spano, F. C. The Spectral Signatures of Frenkel Polarons in H- and J-Aggregates. *Acc. Chem. Res.* **2010**, *43* (3), 429–439. <https://doi.org/10.1021/ar900233v>.
- (42) Son, M.; Park, K. H.; Shao, C.; Würthner, F.; Kim, D. Spectroscopic Demonstration of Exciton Dynamics and Excimer Formation in a Sterically Controlled Perylene Bisimide Dimer Aggregate. *J. Phys. Chem. Lett.* **2014**, *5* (20), 3601–3607. <https://doi.org/10.1021/jz501953a>.
- (43) Haldar, R.; Mazel, A.; Krstić, M.; Zhang, Q.; Jakoby, M.; Howard, I. A.; Richards, B. S.; Jung, N.; Jacquemin, D.; Diring, S.; Wenzel, W.; Odobel, F.; Wöll, C. A de Novo Strategy for Predictive Crystal Engineering to Tune Excitonic Coupling. *Nat. Commun.* **2019**, *10* (1), 2048. <https://doi.org/10.1038/s41467-019-10011-8>.
- (44) Andrieux, C. P.; Savéant, J. M. Electron Transfer through Redox Polymer Films. *J. Electroanal. Chem.* **1980**, *111* (2–3), 377–381.
- (45) Chuang, C.-H.; Li, J.-H.; Chen, Y.-C.; Wang, Y.-S.; Kung, C.-W. Redox-Hopping and Electrochemical Behaviors of Metal–Organic Framework Thin Films Fabricated by Various Approaches. *J. Phys. Chem. C* **2020**, *124*, 20854–20863. <https://doi.org/10.1021/acs.jpcc.0c03873>.
- (46) Liberman, I.; Shimoni, R.; Ifraemov, R.; Rozenberg, I.; Singh, C.; Hod, I. Active-Site Modulation in an Fe-Porphyrin-Based Metal–Organic Framework through Ligand Axial Coordination: Accelerating Electrocatalysis and Charge-Transport Kinetics. *J. Am. Chem. Soc.* **2020**, *142* (4), 1933–1940. <https://doi.org/10.1021/jacs.9b11355>.
- (47) Li, R.; Li, K.; Wang, G.; Li, L.; Zhang, Q.; Yan, J.; Chen, Y.; Zhang, Q.; Hou, C.; Li, Y.; Wang, H. Ion-Transport Design for High-Performance Na<sup>+</sup>-Based Electrochromics. *ACS Nano* **2018**, *12* (4), 3759–3768. <https://doi.org/10.1021/acsnano.8b00974>.
- (48) Schröder, U.; Oldham, K. B.; Myland, J. C.; Mahon, P. J.; Scholz, F. Modelling of Solid State Voltammetry of Immobilized Microcrystals Assuming an Initiation of the Electrochemical Reaction at a Three-Phase Junction. *J. Solid State Electrochem* **2000**, *4* (6), 314–324. <https://doi.org/10.1007/s100080000130>.
- (49) Genies, E. M.; Pernaut, J. M. Spectroelectrochemical Studies of the Redox and Kinetic Behaviour of Polypyrrole Film. *Synthetic Metals* **1984**, *10* (2), 117–129. [https://doi.org/10.1016/0379-6779\(84\)90087-0](https://doi.org/10.1016/0379-6779(84)90087-0).
- (50) Bessinger, D.; Muggli, K.; Beetz, M.; Auras, F.; Bein, T. Fast-Switching Vis–IR Electrochromic Covalent Organic Frameworks. *J. Am. Chem. Soc.* **2021**, *143* (19), 7351–7357. <https://doi.org/10.1021/jacs.0c12392>.